Slow Crack Growth in Zirconia Ceramics with Different Microstructures

Jérôme Chevalier, Laurent Gremillard, Rachid Zenati, Yves Jorand, Christian Olagnon, Gilbert Fantozzi

SLOW CRACK GROWTH IN ZIRCONIA CERAMICS WITH DIFFERENT MICROSTRUCTURES

J. Chevalier, L. Gremillard, R. Zenati, Y. Jorand,
C. Olagnon and G. Fantozzi

INSA de Lyon, GEMPPM, MR CNRS 5510,
20 avenue Albert Einstein, 69621 Villeurbane Cedex, FRANCE

ABSTRACT

A review of Slow Crack Growth experiments conducted in the same laboratory with the same technique (Double Torsion) is presented for zirconia ceramics with different microstructures: (i) a single crystal cubic zirconia as a model brittle material, (ii) different 3%mol. Yttria Stabilised TZP ceramics with grain sizes in the range of 0.3 to 1 μm with or without grain boundary glassy phase, (iii) a 10%mol. Ceria Stabilised Zirconia with a grain size of about 2 μm and a very high transformation toughening capability, (iv) a multiplex zirconia based composite.

Zirconia materials are susceptible to Slow Crack Growth (SCG) under static stress intensity factors even much lower than the toughness K_{IC}. The analysis of the crack velocity versus stress intensity factor (V-K_I) law shows that SCG is driven by a stress assisted corrosion at the crack tip. The crack resistance increases with the transformation toughening capability: a shift toward high stress intensity factors is observed when going from the single crystal to the Y-TZP and then to the Ce-TZP. The presence of an intergranular glassy phase is analysed. Multiplex zirconia based composites exhibit also other reinforcement mechanisms: enlargement of the transformed zone and crack deflection at the interface between the different layers. They present exceptional crack resistance behaviour.

Key words: Crack, Stress Corrosion, Toughness, Transformation, R-Curve.

1. INTRODUCTION

The concept of stress induced phase transformation in zirconia ceramics represents one of the most remarkable innovations in the ceramic field. Indeed, it was shown in the 70's first by Garvie et al. [1] then by Gupta et al. [2] that zirconia exhibited a transformation toughening mechanism acting to resist to crack propagation. The stress induced phase

transformation involves the transformation of metastable tetragonal grains towards the monoclinic phase at the crack tip which, accompanied by a volumetric expansion, leads to compressive stresses acting to reduce the driving force for crack propagation. Zirconia ceramics can be found in the form of tetragonal zirconia polycrystals (TZP), stabilised in the tetragonal symmetry by an addition of different oxides, for example Cerium (Ce-TZP) or Yttrium (Y-TZP) oxides. Zirconia ceramics can also exist in the form of tetragonal precipitates in a cubic matrix. An example is the Magnesia Partially Stabilised Zirconia, as referred to as Mg - PSZ. ZrO_2 can also be used as one of the components in a composite material, as ZrO_2 dispersed ceramics. An example of such a composite would be the Al_2O_3 - ZrO_2 composites (ZTA). Zirconia can also be found in the form of single crystals for optical properties. In these later, the cubic structure is stabilised by 10 mol.% Yttria and no phase transformation occurs. An extensive number of studies has led to optimal processing routes for increasing the toughness of zirconia based ceramics. It is well recognised that zirconia ceramics can exhibit a toughness from 6 MPa$\sqrt{m}$ for the 3Y-TZP or the ZTA composites to more than 15 MPa$\sqrt{m}$ for the Ce-TZP or some Mg-PSZ which demonstrate a high toughening capability [3]. These fracture toughness values are much higher than the 1.5 MPa$\sqrt{m}$ measured for zirconia single crystal [4].

Ceramics are generally susceptible to slow crack growth (SCG) under static loading which can cause delayed failure. Theoretical and experimental studies in glass or in single crystals (especially sapphire) have shown that SCG was a consequence of corrosion assisted by high stresses at the crack tip, as referred as to stress corrosion [5-12]. Such a stress corrosion is believed to occur in zirconia based ceramics [13-15]. The analysis of SCG in these materials is however difficult due to the effect of transformation toughening on crack velocities. This is the aim of this paper to compare the SCG behaviour of different zirconia materials, with different microstructures, thus with different toughening capabilities. This paper therefore summarises different SCG laws obtained in the same laboratory, mainly with the same Double Torsion (DT) technique. This work is an attempt to show that the SCG behaviour of all zirconia based ceramics is basically the same, i.e. stress corrosion by water molecules at the crack tip, the observed difference lying on the toughening capability of a given zirconia.

2. MATERIALS AND EXPERIMENTAL PROCEDURE

2.1. Experimental procedure: the Double Torsion method

The Double Torsion (DT) was used as a direct method to study Slow Crack Growth in the different zirconia ceramics. The geometry of the DT specimen, the loading configuration and the analysis of experimental results are given in details in refs [16-17] and also in ref [18] in the same proceedings. The experimental results were obtained from either relaxation tests (for the determination of crack velocities higher than 10^{-7} m/s) or constant loading method (for crack velocities lower than 10^{-7} m/s). The method has been compared with indirect methods on micro-cracks in 3Y-TZP and gives an excellent agreement with the latter [19]. The advantage of the DT configuration is to visualise directly the crack extension at the surface of the specimen, and the overall shape of the V-K_I (crack velocity versus applied stress intensity factor) can be obtained without any assumption. Some results are presented for laminate zirconia based composites. They were obtained with the SENB method.

2.2. Materials

Cubic Zirconia Single Crystal:

A 10%mol. Yttria stabilised zirconia single crystal (Marketec inc.) was chosen as a model brittle material, without any reinforcement due to transformation toughening. Only limited literature has been devoted to the study of mechanical properties of zirconia single crystal, because the properties of interest are optical. However, it was found by Pajares et al. [4] that zirconia single crystal fracture characteristics were anisotropic. The toughness measured by the SENB (Single Edge Notched Beam) method varied from 1.5 to 1.9 MPa$\sqrt{m}$ along <110> or <100> direction respectively. Well defined indentation cracks were observed along <110> direction. Thus, it is believed that this latter is a privileged cracking direction. DT specimens were therefore oriented along the <110> direction, the {100} plane corresponding to the specimen plane.

3Y-TZP Ceramics:

3%mol. Yttria stabilised zirconia ceramics present outstanding mechanical properties, especially strength which can reach more than one GPa. These very important strength values obtained for 3Y-TZP are a combination of high toughness (about 6-7 MPa$\sqrt{m}$) and very fine grain size (0,5 μm for most commercial products). Thus, it was considered in this study as another model material, with a small grain size (no or little bridging) and a moderate amount of transformation toughening.

Two commercial powders were used as starting materials. Tosoh co-precipitated powder TZ3Y (Tosoh inc.) was chosen as a highly pure zirconia, with less than 100 ppm impurity content. Daiichi powder was chosen because it exhibits naturally a significant amount of alumina and Silica content (total 1500 ppm) that are beneficial for ageing properties. The powders were elaborated by a slip casting method, all with a 80 wt. % solid content. 2.5 wt. % Colloidal silica was added in one slurry of Tosoh powder in order to achieve a zirconia ceramic with a significant amount of silica phase. The different slurries were put in plaster moulds to eliminate water, then dried at 25°C during 7 days, and fired at different temperatures (heating rate 100°C/h) during 5 hours in air in order to achieve different grain sizes. Table 1 summarises the different zirconia ceramics that were elaborated in this work and the firing conditions. By choosing two different powders, with or without silica addition and by firing at different temperatures, it was possible to process 3Y-TZP with different microstructures, thus different mechanical properties.

Table 1. Nomenclature of the different processed 3Y-TZP ceramics.

Designation	Powder	Firing T°	Grain size	Density
$T_{0.3\mu m}$	Tosoh	1400°C	0.3 μm	> 98 %
$T_{0.5\mu m}$	Tosoh	1450°C	0.5 μm	> 98 %
$T_{1.0\mu m}$	Tosoh	1550°C	1.0 μm	> 98 %
$T\text{-}S_{0.3\mu m}$	Tosoh + 2.5 wt.% SiO_2	1400°C	0.3 μm	> 98 %
$D_{0.3\mu m}$	Daiichi	1350°C	0.3 μm	> 98 %

Ce-TZP Ceramics:

Ce-TZP ceramics present a large amount of tranformation toughening, and fracture toughness up to 15-20 MPa$\sqrt{m}$ were reported. Thus, it was interesting to study the SCG in this crack resistant zirconia ceramic in comparison to 3Y-TZP with a much more limited transformation capability, or to the single crystal without any transformation. Multilayer zirconia based composites were introduced by Marshall et al [20-22] who estimated that the

fracture toughness could be increased, if the length of the transformation zone was restricted to approximately the zone width, which is not the case for monolithic Ce-TZP. They proposed to change the frontal zone in Ce-TZP by introducing laminar composites, containing layers of Ce-ZrO_2 and either Al_2O_3 or mixture of Al_2O_3 and Ce-ZrO_2. They used a colloidal method that allowed formation of layers with thickness as small as 10 μm. In such conditions, a fracture toughness of more than 30 MPa.$m^{1/2}$ was predicted. Thus our aim was to process some laminar composites by slip casting method to investigate the extend of crack resistance of this new generation of materials in comparison to the monolith.

Slip casting by pressure filtration route was used to elaborate: (i)- Dense Ceria Stabilised Zirconia (10%mol. Ce-TZP). (ii)- Multilayer composites based on Ce-TZP. Multilayer composites with alternate layers of dense Ce-TZP and mixture of 20 wt. % Al_2O_3 and 80 wt. % Ce-ZrO_2 were fabricated by sequential slip casting.

The starting materials were: (i) Ce-TZP powder (10 mol% CeO_2) with a mean particle size d_{50} = 0.5μm (Mandoval / Zirconia Sales Ltd CEZ-10, U.K.), and a specific surface area 20 m^2/g (BET), (ii) α-Al_2O_3 powder with d_{50} = 0.3 μm (Baïkowski SM8, France), and a specific surface area 10 m^2/g (BET). Two different aqueous slips containing either Ce-TZP or mixed composition of 80 wt% Ce-TZP and 20 wt% Al_2O_3 with a solid content of 70 wt% were prepared after homogenisation in zirconia or alumina ball mill for 24h at pH 9. Those suspensions were casted in a filtration device with rectangular aluminium mould. The green compacts were dried during one week at 25°C and fired at 1450°C for 1h in air, at a heating rate of 100°C/h.

Full density (> 99% theoretical density) and 1-2 μm grain size were obtained.

The following mechanisms have been identified as active in the toughening of Ce-TZP systems: transformation shielding for the monolith, and interfacial mechanisms (i.e. crack deflection and delamination) for composites. The enlargement of the process zone is also efficient to shield the crack. The crack propagation behaviour of multilayer ceramics were determined at room temperature using SENB experiments, because DT is not adapted in this last case, due to the curve crack front which would complicate the analysis.

3. RESULTS AND DISCUSSION

3.1. Slow Crack Growth by stress corrosion in zirconia ceramics

Different systematic studies on Slow Crack Growth have been conducted on glass, alumina single crystals and mica [5-12]. As a general trend, they have shown that an unique relation could be established, for a given environment, between the velocity (V) and the stress intensity factor (K_I) with three different stages attributed to distinct mechanisms. In the first stage (Region I, for low velocities), crack propagation is limited by the thermally activated reaction kinetic between the ceramic and corrosive molecules. These molecules were clearly identified in the case of silica as H_2O [5]. Region II, at intermediate velocities, depends on environment, but is much less sensitive to K_I. This region is often attributed to gaseous diffusion along the crack interface. Region III, for high velocities represents the fracture of ceramic bonds without chemical reaction with environmental species. Although mentioned by Wiederhorn [7] in glass, the occurrence of a threshold is still under debate. Recently, Wan et al. [23-24] considered this point and the presence of a threshold was definitely shown in mica. These authors and Maugis [25] considered that the threshold corresponds to an equilibrium with a null crack velocity. In this respect, crack healing should occur below the threshold, which was partly shown in the case of mica [24].

A large number of studies have focused on SCG in zirconia ceramics. However, there is only a sparse collection of data where the crack rate versus the applied stress intensity

factor (V-K_I) has been obtained for a large range of crack rates. Knechtel et al. [13] have obtained V-K_I curves for Y-TZP and Al_2O_3 / Y-TZP ceramics in the crack velocity regime from 10^{-12} m/s to 10^{-2} m/s. Their measurements have been confirmed and completed by Chevalier et al. [19] for a 3Y-TZP in different atmospheres with more experimental data. The V-K_I diagram for a commercial 3Y-TZP zirconia ceramic (Supplied by Norton Desmarquest Fine Ceramics, France), with a grain size of 0.5 μm is presented in Figure 1 for different environments. The overall curve in air presents three different stages and a threshold value K_{IO} below which no propagation takes place. In water, only one stage is observed and the slope of the curve is similar to that of the first stage in air. It is important to point out the results in silicon oil or under vacuum where no water molecules are present: the V-K_I curve presents a much higher slope and SCG operates only for stress intensity factors near K_{IC}. These results suggest that a stress corrosion mechanism operates, as in glass or in monocrystalline ceramics. This is supported by the increase of crack velocities in water when the temperature increases. The first stage in air can be fitted by a power law:

$$V = A \cdot K_I^n \qquad (1)$$

where A and n are constants dependent on the material properties. Chevalier et al. [19] have found a value for n of about 32 for 3Y-TZP ceramics with different grain sizes and Knechtel et al. [13] have found 29 and 44 for their materials. The value for K_{I0} was determined to 3.5 MPa√m in air, 3.1 MPa√m in water and 4.9 MPa√m under vacuum conditions. A systematic study on the effect of temperature on crack velocities has lead to an activation energy of 70 KJ/mol.

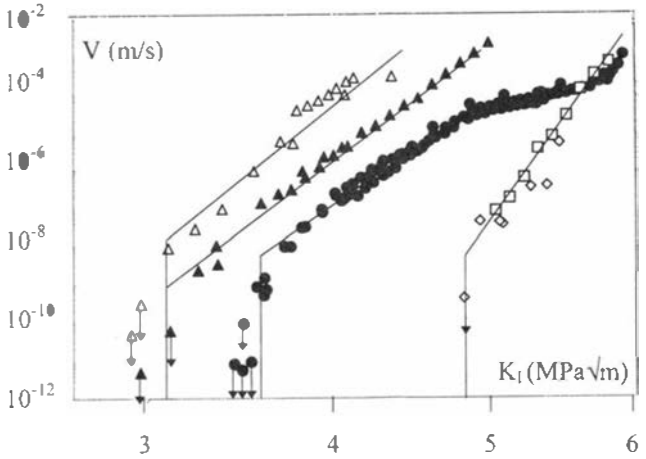

Figure 1. V-K_I law for a commercial 3Y-TZP ceramic with a grain size of 0.5 μm (from ref [19]). ● : air, 25°C ; ▲: distilled water, 25°C ; Δ : distilled water, 75°C ; □ : silicon oil, 25°C ; ◊: secondary vacuum, 25°C.

3.2. Effect of transformation toughening and the presence of a glassy phase on Slow Crack Growth in 3Y-TZP

Figure 2 represents the V-K_I laws obtained for the different 3Y-TZP ceramics and for single crystal. The data for silica glass obtained with the same DT technique are also plotted, they will be discussed further. Regarding the results for the 3Y-TZP, it is clear that an increase in the grain size leads to a shift towards the high stress intensity factors,

expressing an increase of crack resistance due to higher transformability. In comparison with zirconia single crystal (and silica), V-K_I curves for polycrystalline 3Y-TZP are shifted towards much higher stress intensity factors. It is obviously a consequence of transformation toughening that act to shield the crack from the external driving force. It is however interesting to note that all the curve, even for the single crystal ceramic, exhibit three distinct stages corresponding to the three stress corrosion propagation stages discussed above. The second stage, which corresponds to the gaseous diffusion of water molecules inside the crack path occurs for the same crack rates ($\sim 10^{-4}$ m/s). In terms of stress intensity factor, the stress – induced transformation leads to a shielding K_{Ish} according to:

$$K_I = K_{Itip} + K_{Ish} \tag{2}$$

where K_{Itip} is the local crack tip stress intensity factor and K_I the external applied stress intensity factor.

The shielding stress intensity factor in toughened ceramics with a regular zone shape has been evaluated as [26]:

$$K_{Ish} = C_{sh} \cdot K_I \tag{3}$$

with

$$C_{sh} = \frac{0.214 \cdot E \cdot V_f \cdot e^T \cdot (1+\nu)}{(1-\nu) \cdot \sigma_m^c} \cdot \left(\frac{\sqrt{3}}{12\pi}\right) \tag{4}$$

where E is the Young modulus, V_f the volume fraction of transformed particles, e^T is the volume dilatation associated to the transformation, ν the Poisson ratio, $\sigma_m{}^c$ is the local stress for phase transformation and K_I the applied stress intensity factor. Eqn (3), which suggests that the shielding stress intensity factor is proportional to the applied one, has been verified experimentally by Chevalier et al. [19] and Alcala et al. [27]. Reporting Eqn (3) in Eqn (2), the stress intensity factor at the crack tip, K_{Itip}, can be expressed as:

$$K_{Itip} = (1 - C_{sh})K_I \tag{5}$$

C_{sh} increases with the material transformability. If we assume that the intrinsic mechanism of SCG at the crack tip is the same for all zirconia ceramics, i.e the fracture of the zirconia bonds (or the silica bonds present in the intergranular vitreous phase) by water molecules, the crack rate must always been given by:

$$V = A_0 \cdot K_{Itip}{}^n \tag{6}$$

Therefore, the experimentally determined V-K_I law is:

$$V = A_o \cdot \left(1 - C_{sh}\right)^n \cdot K_I{}^n = A \cdot K_I{}^n \tag{7}$$

From Eqn (5), it can be argued that the intrinsic toughness K_{ICtip} (the toughness we would measure if there was no transformation toughening) is related to the experimental toughness K_{IC} by:

$$K_{ICtip} = (1 - C_{sh})K_{IC} \tag{8}$$

By reporting Eqn (8) in Eqn (7), one obtains:

$$V = A_o \cdot \left(K_{ICtip}\right)^n \cdot \left(\frac{K_I}{K_{Ic}}\right)^n \tag{9}$$

Therefore the rationalisation of the V-K_I curves by the experimentally determined toughness K_{IC} must lead to the same 'master curve', whatever the microstructure. This plot should depend only on the intrinsic V-K_{Itip} law of a given ceramic. This V-(K_I/K_{IC}) plot is presented in Figure 3.

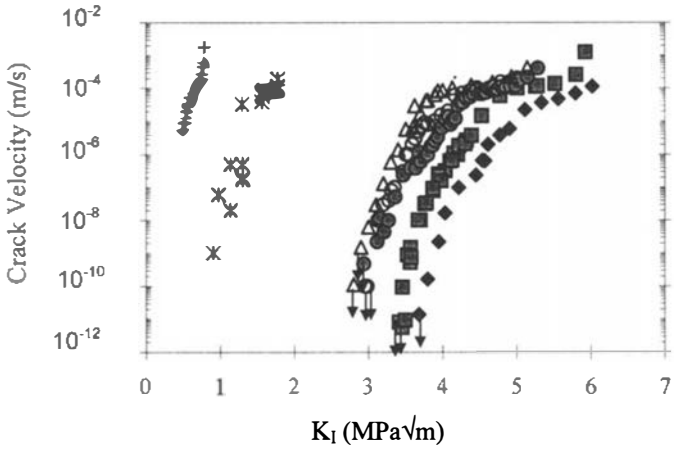

Figure 2. V-K_I laws obtained for different 3Y-TZP zirconia ceramics compared to single crystal and silica. ◆ : $T_{1.0\mu m}$; ■ : $T_{0.5\mu m}$; ● : $T_{0.3\mu m}$; ○ : T-$S_{0.3\mu m}$; △ : $D_{0.3\mu m}$; * : zirconia single crystal ; + : silica glass.

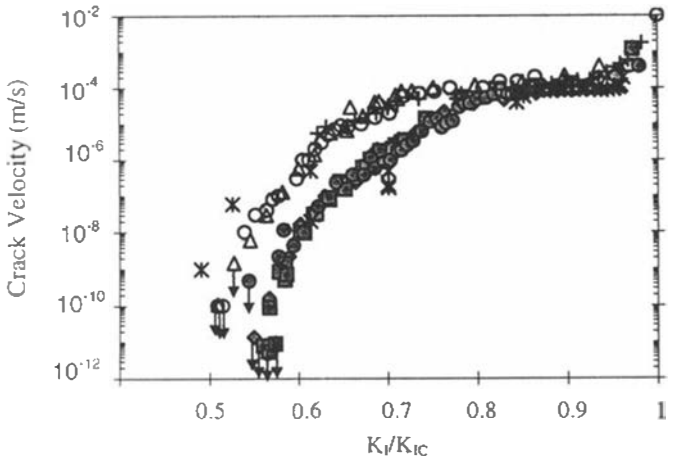

Figure 3. Rationalised V-K_I/K_{IC} laws of the different ceramics (same symbols than for Figure 2).

The different zirconia ceramics exhibit nearly the same rationalised V-K_I/K_{IC} curves. However, there is a significant difference between ultra pure 3Y-TZP ceramics ($T_{0.3\mu m}$, $T_{0.5\mu m}$, $T_{1.0\mu m}$) and 3Y-TZP exhibiting silica (and alumina) in the starting powder ($D_{0.3\mu m}$

and T-$S_{0.3\mu m}$). Of importance is the coincidence between zirconia single crystal and the former and between silica and the latter. This could traduce a fracture of zirconia bounds in the case of pure 3Y-TZP ceramics and a significant amount of fracture of silica bounds for the less pure 3Y-TZP.

Transmission Electron Microscopy (TEM) analysis was achieved on the different 3Y-TZP in order to investigate the presence of an amorphous silica rich grain boundary phase, which should appear in zirconia ceramics as mentioned earlier by several authors. All pure zirconia ceramics (processed with the ultrapure Tosoh powder) exhibit any grain boundary phase, neither at the grain boundary nor at triple points, as shown in Figure 4.a and 4.b in $T_{0.5\mu m}$. In contrast, $D_{0.3\mu m}$ exhibited a thin amorphous layer of about 1nm or less (cf Figure 5.a), which is in agreement with the value predicted by Clark [28]. The presence of amorphous triple points was also observed for this ceramic (Figure 5.b). Energy Dispersive Spectroscopy revealed the presence of silica and alumina in the grain boundaries. At last, T-$S_{0.3\mu m}$, which was processed from Tosoh powder and an addition of colloidal silica, exhibited a important number of large glassy triple points (Figure 6). However, the presence of silica rich glassy phase at the grain boundary was not clear, and most of the observed grain boundaries were clean.

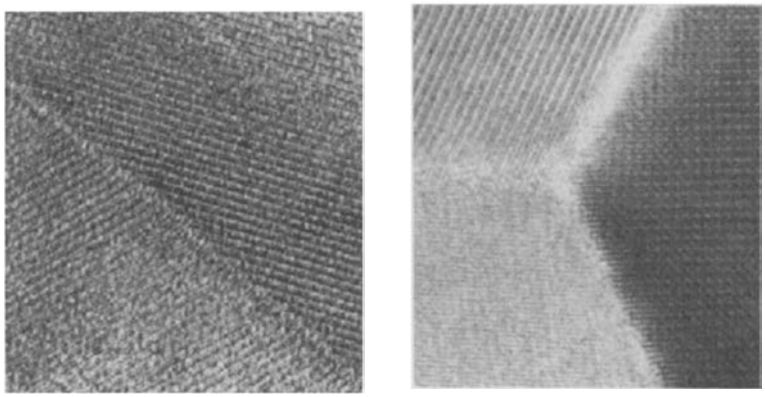

(a) (b)

Figure 4. Grain boundaries and triple points for $T_{0.5\mu m}$ without any glassy phase.

Thus, the effect of grain size and of the presence of a grain boundary glassy phase is obvious from the theoretical analysis developed above and from the different results :

(i) an increase of the grain size leads to increased crack resistance according to Equations (3) and (4) where σ^m_c decreases when the grain size increases.

(ii) The presence (even partial) of a glassy phase at the grain boundary and/or at the triple junctions between grains leads to a combination of fracture of silica bounds and zirconia bounds, instead of zirconia bounds only for pure zirconia ceramics. The intrinsic propagation law is changed in the presence of silica, and thus the V-K_I/K_{IC} law is not the same. However, the difference between 'pure' and SiO_2 doped 3Y-TZP is not very important because of transformation shielding that act to increase crack resistance in all cases.

It is to note that such rationalisation has been conducted for other results on different types of zirconia ceramics from the literature in zirconia by Chevalier et al. [29].They have concluded that all zirconia based ceramics exhibit approximately the same 'master' V-K_I/K_{IC} law under both static and cyclic fatigue.

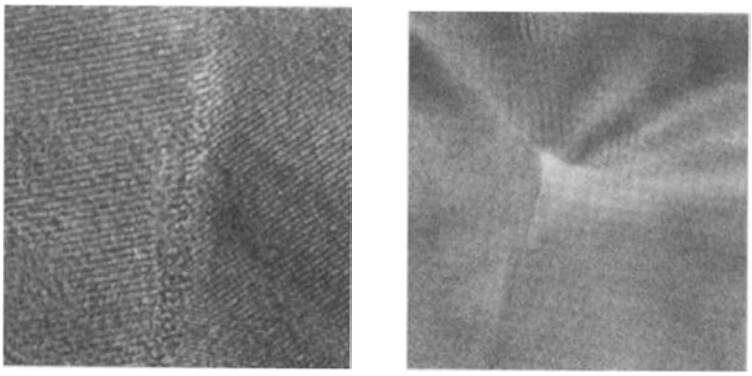

(a) (b)

Figure 5. Presence of a thin amorphous glassy layer in a grain boundary and at a triple point in $D_{0\text{-}3\mu m}$.

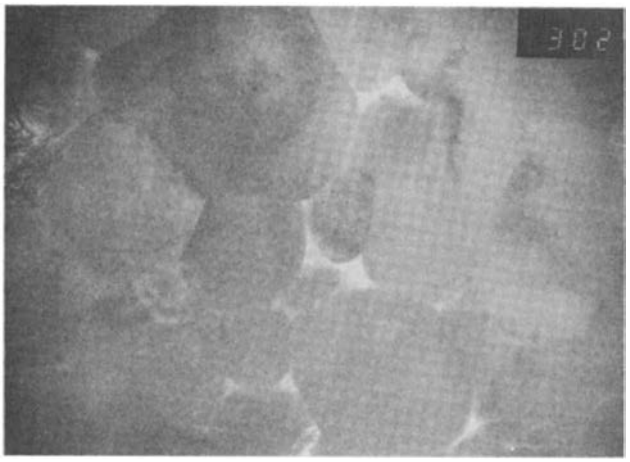

Figure 6. Numerous glassy phase pockets at triple points in $T\text{-}S_{0.3\mu m}$. Note the rounded shape of grains. However, the presence of silica rich glassy phase at the grain boundary was not clear.

3.3. Modelling of Slow Crack Growth in zirconia ceramics

The treatment of environment-sensitive crack velocity in ceramics by stress corrosion models has been widely documented for single crystal ceramics or glass [9]. Formulations for the crack velocity in the three regions should be written :

Region I:

$$V_I = 2 \cdot \nu_0 \cdot a_0 \cdot \exp\left(-\frac{E_{0I}}{kT}\right) \cdot \sinh\left[\frac{\alpha_I \cdot (G^* - 2\gamma)}{kT}\right] \qquad (10)$$

Region II:

$$V_{II} = \frac{64 \cdot G^*}{3 \cdot \pi \cdot E \cdot a_0 \cdot \ln\left(\frac{l}{a_0}\right)} \cdot \frac{{a_0}^3 \cdot p_E}{\sqrt{(2 \cdot \pi \cdot m \cdot kT)}} \qquad (11)$$

Region III:

$$V_{III} = 2 \cdot \nu_0 \cdot a_0 \cdot \exp\left(-\frac{E_{0III}}{kT}\right) \cdot \sinh\left[\frac{\alpha_{III} \cdot (G^* - 2\gamma s)}{kT}\right] \qquad (12)$$

where G* is the net crack tip driving force for crack propagation, i.e. $G-G_{sh}$, G_{sh} being the effect of reinforcement on crack tip driving force.

In these equations, υ_o is the Boltzmann frequency, a_0 the bond spacing, k the Boltzmann constant, γ and γs the surface energy in the presence or absence of water molecule respectively, T the absolute temperature. The bond spacing for zirconia can be taken as $a_0=a/2\sqrt{2}$ where a is the lattice parameter, about 0.5 nm, for a crack propagation through <110> direction. E_{OI} and E_{OIII} are the activation energy of stress corrosion in region I and region III. α_I and α_{III} traduce the stress dependence of crack velocity. Region II is related to the diffusion controlled stage of crack propagation, m is therefore the mass of water molecules and p_E the water pressure. The first term of equation (11) incorporates the pressure differential between the mouth (source) and tip (sink) which regulates the flow rate, so l represents the crack opening displacement, on the order of 1μm. E is the Young modulus, 220 GPa for zirconia ceramics.

G* can be calculated directly from G. Indeed, in the case of zirconia single crystal, G*=G because no microstructural reinforcement occurs. In the case of zirconia polycrystals, the contribution of shielding can be estimated from Equation (5) by a comparison of the V-K_I law for a given polycrystal and for the single crystal. For all the velocities measured, the applied K_I and the intrinsic K_{Itip} were proportional. The constant C_{sh} has been calculated for the three grain sizes investigated in this work. This gives a proportionality factor between the applied driving force G and the crack tip driving force G* by:

$$G = \frac{K_I^2}{E} = \frac{K_{Itip}^2}{E \cdot (1 - C_{sh})^2} = \frac{1}{(1 - C_{sh})^2} \cdot G^* = \frac{1}{C_{Gsh}} \cdot G^* \qquad (13)$$

Table 2 gives this proportionality factor as a function of the grain size.

Table 2.

Grain size	0.3 μm	0.5 μm	1.0 μm
C_{Gsh}	0,128	0,104	0.0865

The fit of experimentally determined V-G* laws by the three stress corrosion equations are shown in Figure 7. In this fit, it was considered that region I and II act in series and that region II and region III are parallel mechanisms.

The different parameters α_I, α_{III}, γ, γs, E_{OI} and E_{OIII} deduced from this plot are summarised in Table 3. They can be used to predict V-G* function of zirconia in any environmental condition.

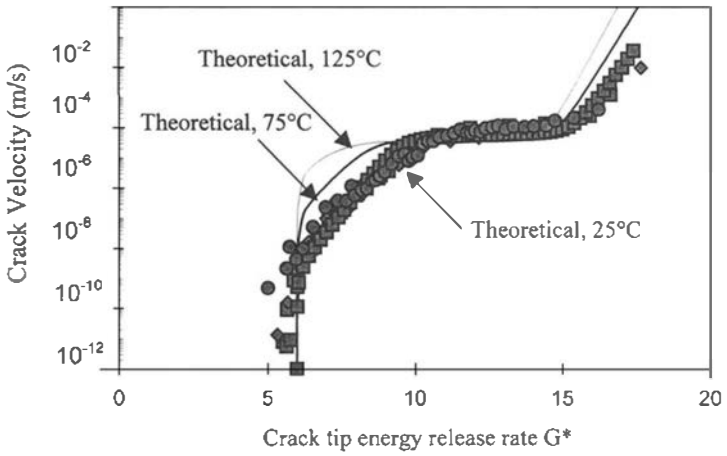

Figure 7. Intrinsic V-G* law of pure zirconia ceramics. ◆: $T_{1.0\mu m}$; ■: $T_{0.5\mu m}$; ●: $T_{0.3\mu m}$.

Figure 8 shows the V-G* laws of the different zirconia ceramics, with or without glassy phase, in comparison with silica glass and zirconia single crystal. Even for D0.3µm and T-S0.3µm, the V-G* law is much nearer from the single crystal zirconia than for silica glass. This should indicate that all the grain boundaries are not wetted by the glassy phase and that a significant proportion of fracture occurs also for zirconia bounds. As fracture occurs more easily for silica than for zirconia bounds, the lowest step in the chain should rule the overall crack velocity. It is also important to note that the real composition of the glassy phase is not known exactly and can differ from that of the silica glass tested in the present work.

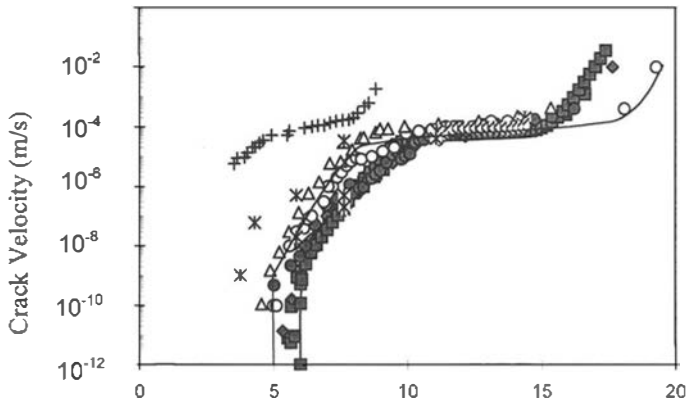

Figure 8. V-G* laws for all 3Y-TZP as compared to silica glass.
◆: $T_{1.0\mu m}$; ■ : $T_{0.5\mu m}$; ●: $T_{0.3\mu m}$; ○: $T\text{-}S_{0.3\mu m}$; Δ: $D_{0.3\mu m}$; ✻ : zirconia single crystal ; + : silica glass.

Table 3.

γ	γs	α_I/k	α_{III}/k	E_{OI}	E_{OII}
3	6	850	1200	70 KJ/mol.	***

3.4. Crack Growth in Ce-TZP: importance of the R-Curve on Slow Crack Growth.

Modelling of SCG in 3Y-TZP with stress corrosion and transformation toughening models was possible, because stress-assisted phase transformation zones were limited. Indeed, it was shown by several authors that the zone with in 3Y-TZP was less than 10 μm [15]. Thus, the R-Curve of 3Y-TZP ceramics is rising steeply over the first tens of microns then becomes constant [30]. This means that DT results obtained in 3Y-TZP were obtained on the plateau of the R-Curve. Equation (4) is only valid on this plateau, which is not the case for Ce-TZP with an R-Curve rising over several millimetres. Figure 9 represents the transformation zone observed in the Ce-TZP ceramic, on the surface of a DT specimen. The zone width is about 100 μm and the zone length reaches several hundreds of microns (~1500 μm).

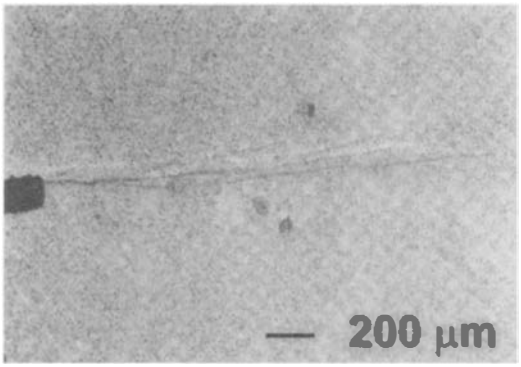

Figure 9. Transformation zone in 10wt.% mol Ce-TZP.

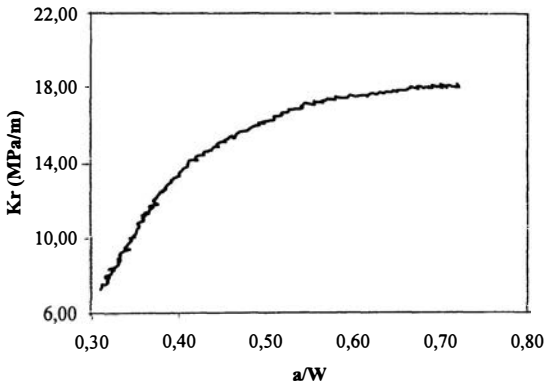

Figure 10. Crack resistance (K_R) versus relative crack length (a/W, with W: specimen height of 6 mm) of Ce-TZP measured by SENB method.

This leads to extensive crack resistance, as represented in Figure 10 for a measurement with the SENB method: the toughness reaches 18 MPa$\sqrt{m}$ after several hundreds of microns extension, and we remember that the intrinsic toughness of zirconia is of 2 MPa$\sqrt{m}$. Of importance is also the load-displacement curve obtained by DT for the Ce-TZP material on Figure 11 which shows an extensive non-linear behaviour, in comparison with more common brittle ceramics.

Acoustic Emission can be monitored during the loading of a specimen. It was shown by Gogotsi et al. [31] that Acoustic Emission was generally observed before crack propagation, traducing extensive transformation even before crack extension. This was verified in our experiments both by SENB and DT methods. At last, a number of secondary cracks were observed that act also to reduce the crack tip driving force.

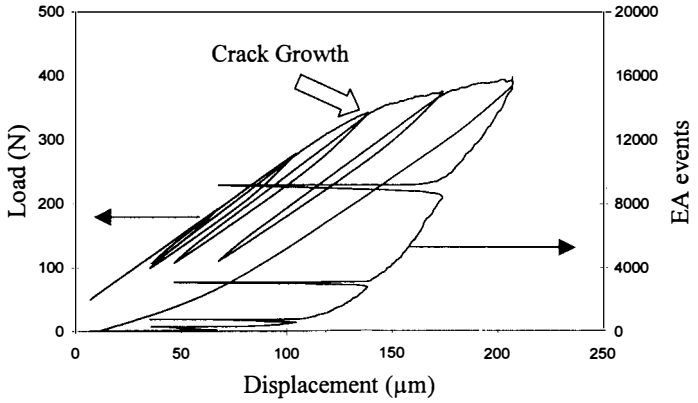

Figure 11. Load – displacement curve for Ce-TZP measured with the DT method.

The DT was used to identify the Slow Crack Growth behaviour of the Ce-TZP ceramic. Two successive relaxation tests were conducted on the same specimen. The analysis of the tests was made with a compliance analysis, as described in [18] in this series of proceedings. As shown in Figure 12, The V-K_I law depends drastically on the crack length, as a consequence of increasing crack shielding. The V-K_I law is shifted towards higher stress intensity factor values as the crack advances. This effect has been analysed in details for alumina in ref [18]. It however more pronounced for Ce-TZP as a consequence of a much stronger R-Curve behaviour. The second relaxation corresponds to the plateau of the R-Curve and Slow Crack Growth occurs for applied stress intensity factors near 18 MPa$\sqrt{m}$. In this latter experiment, for high applied loads, a spasmodic crack propagation was observed, which was traduced by a complex V-K_I law, with slow down – speed up sequences. This effect which has not been described elsewhere has been attributed to the generation of a secondary crack outside the transformation zone, when the main crack was stopped by the transformation zone. The sudden drop of the load during relaxation tests was always connected to a crack branching: the main crack was slowed down by the transformation, and a secondary crack started at high speed, then again slowed down by another branch of transformation zone.

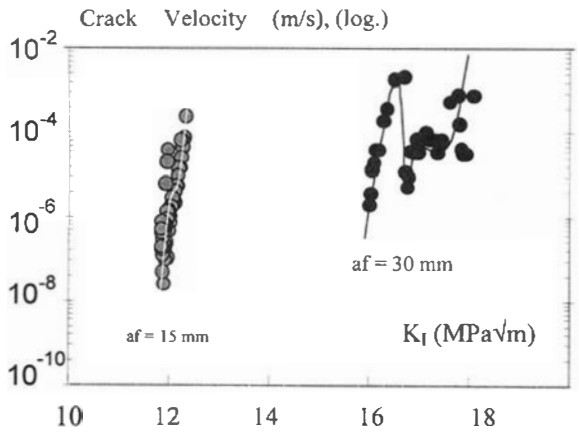

Figure 12. V-K_I law of a Ce-TZP for two successive DT relaxation tests.

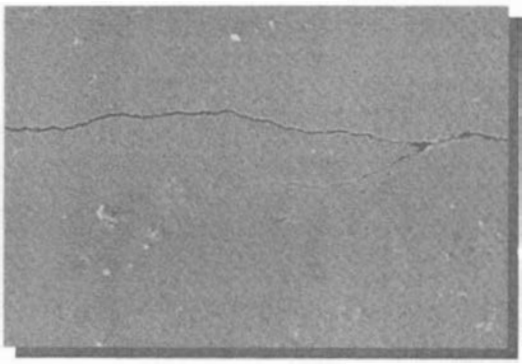

Figure 13. Crack branching observed at each acceleration of the crack rate in the Ce-TZP ceramic.

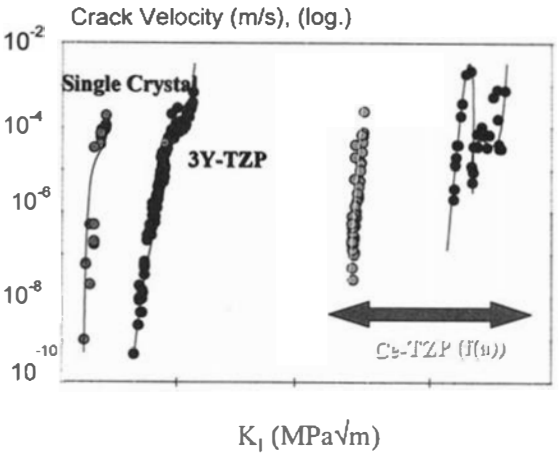

Figure 14. V-KI diagram for the different groups of zirconia ceramics.

Further work is needed to analyse precisely SCG in Ce-TZP ceramics. It would be interesting to suppress the R-Curve behaviour of the material from the experimental SCG results to describe the real intrinsic V-K_{Itip} of this material in comparison with 3Y-TZP or single crystal. However, it is clear that the strong reinforcement in this material, as compared to the single crystal or even to the 3Y-TZP ceramics shows the potential of such a ceramic for load bearing applications, where SCG is of prime importance. Figure 14 represents the V-K_I laws that were obtained in this work for the single crystal, 3Y-TZP ceramic with a 0.5 μm grain size and for the Ce-TZP ceramic. The SCG data spread from 2 to 18 MPa$\sqrt{m}$ for the same basic material, as a consequence of transformation toughening capability.

3.5. Crack propagation in Ce-TZP based composites

High fracture toughness has been achieved for Ce-TZP that undergoes extensive martensitic transformation from tetragonal to monoclinic phase. However, the transformation zones surrounding cracks in this material, tend to extend far ahead of the crack a distance of 10 to 20 times the zone width (cf. Figure 9). The extra transformed material ahead of the crack degrades the toughening. For a steady-state cracking (crack growth at constant K_I), with a zone containing a uniform volume fraction, f, of transformation product over a distance w from the crack surface, the shielding stress intensity factor is:

$$K_{sh} = \frac{A \cdot f \cdot e^T \cdot w^{1/2}}{(1-\nu)} \qquad (14)$$

Where, E is the Young's modulus, ν is the Poisson's ration, e^T is the net dilatation and A is a dimensionless constant dependent on the zone shape ahead of the crack tip. In order to assess the role of the extended frontal zone on crack tip shielding, the shape parameter «A» can be evaluated for any specified zone shape using the weight function method of Mc Meeking et al. [26].

Marshall et al [22] estimated that the fracture toughness could be increased, if the length of the transformation zone was restricted to approximately the zone width, which is the case for magnesia-partially-stabilised zirconia (Mg-PSZ) or 3Y-TZP. They proposed to change the frontal zone in Ce-TZP by introducing laminar composites, containing layers of Ce-ZrO_2 and either Al_2O_3 or mixture of Al_2O_3 and Ce-ZrO_2. They used a colloidal method that allowed formation of layers with thickness as small as 10 μm. In such conditions, a fracture toughness of more than 30 MPa$\sqrt{m}$ was predicted. Our purpose was therefore to still increase the crack resistance of the present Ce-TZP by using this concept. Laminar materials with alternate layers of dense Ce-TZP (A) and a mixture of 80 wt. % Ce-TZP and 20 wt. % Al_2O_3 (B) were fabricated using colloidal technique. The technique involved sequential slip casting by pressure filtration of solution containing suspended particles to form the layered green body followed by drying and natural sintering at 1450°C for 1h. The technique is described in more details in ref [32]. The final materials consisted of different layers (from 3 to 9) in sequences A/B/A/B/A with an overall thickness of 3 mm. Notched beam crack growth experiments were conducted at room temperature. The dimensions of the beams were 30 mm*5 mm*3 mm with an initial notch of 1 mm depth.

The apparent toughness (apparent because the behaviour is far from linear elastic) of the composites can reach values up to 50 MPa$\sqrt{m}$, which is exceptionally high for ceramic based materials. Figure 15 shows a micrograph of a notched composite loaded in flexion. An enlargement of the transformation zone at the first interface is apparent on the micrograph, as well as autocatalic transformation in the last zirconia layer. Strong

delamination and crack deviation was seen at all the interfaces and act for the high toughness of this materials.

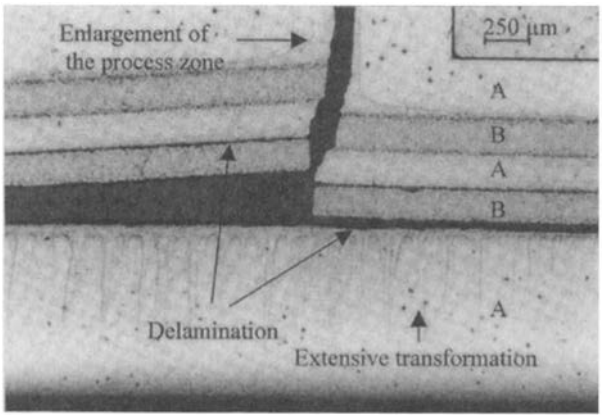

Figure 15. Micrograph of a five layers multiplex zirconia based composite loaded in flexion. Note the different reinforcement mechanisms leading to a toughness of 50 MPa$\sqrt{m}$.

4. CONCLUSION

The Slow Crack Growth behaviour of zirconia ceramics with different microstructures has been analysed.

(i) SCG is a consequence of stress-assisted corrosion at the crack tip by water molecules.

(ii) The effect of transformation toughening is to shift of V-K_I laws towards high stress intensity values, as a consequence of increased crack resistance.

(iii) By taking into account the transformation toughening in the analysis of SCG, it is shown that the intrinsic V-K_{Itip} behaviour of pure 3Y-TZP ceramics is the same than that of single crystal.

(iv) The presence of a glassy phase at the grain boundary or at the triple points changes the V-K_{Itip} law of zirconia ceramics. It leads to a small decrease of crack resistance.

(v) Ce-TZP exhibits a large amount of transformation toughening. Transformation zone spread over hundreds of microns, leading to strong R-Curve behaviour that complicate the SCG analysis. Ce-TZP ceramics can reach very important toughness values for monolithic ceramics.

(vi) By a modification of the transformation shape and with the aid of other reinforcement mechanisms (delamination, crack deviation), it is possible to process zirconia based materials with high reliability.

REFERENCES

1. R.C. Garvie, R.H.J. Hannink and R.T. Pascoe, *Nature*, London, 258, 703-704 (1975).
2. T.K. Gupta, F.F. Lange and J.H. Bechtold, *J. Mater. Sci.*, 13, 1464-70 (1978).

3. D.J. Green, R.H. Hannink and M.V. Swain, *Transformation Toughening of Ceramics*, ed. CRC Press INC., Boca Raton, Florida, 232 (1989).
4. A. Pajares, F. Guiberteau, A.D.Rodriguez, A.H.Heuer, *J. Am. Ceram. Soc.*, 71, 7, C-332-C-333 (1988).
5. T.A.Michalske and S.W.Freiman, *J. Am. Ceram. Soc.*, 66, 4, 284-88 (1983).
6. B.R. Lawn, *J. Am. Ceram. Soc.*, 66, 2, 83-91 (1983).
7. S.M. Wiederhorn, in: NBS special publication, *Mechanical and thermal properties of ceramics*, 303, 217-41 (1969).
8. S.M. Wiederhorn and L.H. Boltz, *J. Am. Ceram. Soc.*, 53, 553 (1970).
9. B.R. Lawn, *Fracture of Brittle Solids*, Second Edition, Cambridge University Press, 380 (1993).
10. T.A. Michalske, B.C. Bunker and S.W. Freiman, *J. Am. Ceram. Soc.*, 69, 10, 721-24 (1986).
11. K.T. Wan, S. Lathabais and B.R. Lawn, *J. Europ. Ceram. Soc.*, 6, 4, 259-68 (1990).
12. B.R.Lawn, *Mater. Sci. and Eng.*, 13, 277-283 (1974).
13. M. Knechtel, D. Garcia, J. Rödel, N. Claussen, *J. Am. Ceram. Soc.*, 76, 6, 2681-84 (1993).
14. J. Chevalier, C. Olagnon, G. Fantozzi, B.Cales, *J. Am. Ceram. Soc.*, 78, 7, 1889-94 (1995).
15. M.M. Nagl, L. Lhanes, R. Fernandez and M. Anglada, in: *Fracture Mechanics of Ceramics, Vol. 12*, R.C. Bradt et al., ed., Plenum Press, New York (1996).
16. J. Chevalier, M. Saadaoui, C. Olagnon, and G. Fantozzi, *Ceram.Inter.*, 22, 171-177 (1996).
17. J. Chevalier, C. Olagnon and G. Fantozzi, in: *Fracture Mechanics of Ceramics, Vol.12*, R.C. Bradt et al., ed., Plenum Press, New York (1996).
18. M. Ebrahimi, J. Chevalier, M. Saadaoui and G. Fantozzi, *ibid.*
19. J. Chevalier, C. Olagnon and G. Fantozzi, *J. Am. Ceram. Soc.*, in press, november (1999).
20. D.B. Marshall, J.J. Ratto, & F.F. Lange, *J. Am. Ceram. Soc.*, 74, 2979-87 (1991).
21. D.B. Marshall, *Ceramic Bulletin*,71, 6, 969-73 (1992).
22. D.B. Marshall, & J.J. Ratto, in: *Science and Technology of Zirconia V*, 517-23 (1993).
23. K.T. Wan, S. Lathabai and B.R. Lawn, *J. Europ. Ceram. Soc*, 6, 4 259-68 (1990).
24. K.T. Wan, N. Aimard and S. Lathabais, *J. Mater. Research*, 5, 1 172-82 (1990).
25. D. Maugis, *J. Mater. Sci.*, 20, 3041-73 (1985).
26. R.M. McMeeking and A.G. Evans, *J. Am. Ceram. Soc.*, 65, 6 242-46 (1982).
27. J. Alcala and M. Anglada, To be published in *J. Am. Ceram. Soc.* (1999).
28. D.R. Clarke, *Ann. Rev. Mater. Sci.*, 54-57 (1987).
29. J. Chevalier, C. Olagnon and G. Fantozzi, *Composites, Part A*, 30, 525-530 (1999).
30. R.M. Anderson and L.M. Braun, *J. Am. Ceram. Soc.*, 73, 10, 3059-62 (1990).
31. G.A. Gogotsi, V.P. Zavada and M.V. Swain, *J. Europ. Ceram. Soc.*, 16, 545-551 (1996).
32. R. Zenati, Ph.D. Thesis, in preparation, INSA de Lyon, France (1999).